MASSACHUSETTS INSTITUTE OF TECHNOLOGY
NAVAL SUPERSONIC LABORATORY

Technical Report 387

INFRARED RADIATION FROM AERODYNAMICALLY HEATED SURFACES

by

Lawrence D. Lorah

June 1959

Massachusetts Institute of Technology
Naval Supersonic Laboratory
Cambridge, Massachusetts

Technical Report 387

INFRARED RADIATION FROM AERODYNAMICALLY HEATED SURFACES

by

Lawrence D. Lorah

Contract No. Nonr 1841(40)

MIT DSR No. 7683

June 1959

ABSTRACT

A theoretical method is presented for determining a spectral and spatial description of the infrared radiation from aerodynamically heated surfaces. The basic laws of infrared emission from opaque surfaces are reviewed and put into a form useful in this application. Heat transfer rates to flat plates and cones in laminar and turbulent supersonic flow are examined and pertinent equations are presented. Solutions for equilibrium temperatures are obtained for representative flight conditions and the radiation laws are applied to produce characteristic radiation patterns at various altitudes and Mach numbers. As an example, the radiation from the skin of a hypothetical aircraft is found for various flight conditions.

TABLE OF CONTENTS

LIST OF ILLUSTRATIONS

LIST OF SYMBOLS

A	Area
c	Speed of propagation of radiation
c_f	Friction coefficient
c_p	Specific heat at constant pressure
F(Z)	Function of Z
h	Planck's constant
h	Heat transfer coefficient
k	Boltzman's constant
K	Thermal conductivity
ℓ	Length
m	Transformed flux
M	Mach number
n	Transformed wavelength
Pr	Prandtl number
q	Flux, (power per unit area)
q_λ	Flux per unit wavelength
r	Recovery factor
R	Range
Re	Reynolds number
St	Stanton number
T	Temperature
u	Velocity
w	Power
x	Distance along stream
Z	Nondimensionalized distance along stream
α	Solar constant
γ	Ratio of specific heats
ϵ	Emissivity
θ	Angle from normal
λ	Wavelength
μ	Viscosity
ν	Kinematic viscosity
ρ	Density
σ	Stefan-Boltzmann constant

Subscripts

av	Average
aw	Adiabatic wall
bb	Black body
i	Incompressible
ℓ	Laminar
s	Sun
t	Turbulent
0	Stagnation
∞	Free stream
max	At q_λ maximum
τ	Effective total
λ	Per unit wavelength

Superscripts

0	Static or ambient
*	Reference temperature

SECTION I
INTRODUCTION

As infrared sensitive devices become of greater and greater importance in aerial warfare, it is imperative that the equipment designer have, at hand, knowledge of target radiation signatures. Even though such considerations as background characteristics and optical design help determine the ultimate capabilities of a detecting or tracking system, one of the most basic pieces of information necessary for intelligent design is the level and spectral distribution of the infrared energy coming from the target. In the case of aerial craft this infrared radiation can come from several sources. The structure becomes heated and the exposed surfaces emit radiation peculiar to their temperature distributions and surface characteristics. The propulsion system produces a strongly radiating plume of gas if it is a jet or rocket system. Sunlight and earth radiation can be reflected from the surfaces, and at very high speeds and at extreme altitudes the heated air layer surrounding the craft and the hot wake may produce significant infrared energy.

The purpose of this paper is to examine the first source of radiation, the aerodynamically heated, external surfaces of the vehicle, and develop satisfactory methods of estimating its level and spectral distribution. It has proven difficult to obtain satisfactory radiation measurements of heated airframes, especially under realistic flight conditions. Even if methods were developed to make accurate measurements on the pertinent vehicles, a potential enemy would not allow measurements to be made on his weapons. Therefore it is necessary to develop engineering methods of predicting the radiation characteristics of these surfaces once adequate target models and operating conditions are established. High accuracy in the calculations is not usually necessary due to the uncertainty in target geometry and operating conditions.

However, care should be taken so that the results obtained are meaningful and should be as accurate as the target characteristic hypothesis.

The problem is approached by first reviewing the basic laws of infrared emission from opaque surfaces in order to clarify nomenclature and to establish useful equations and approximations. Then the heat transfer rates and equilibrium temperatures for the surfaces under consideration are examined. The major mode of the heat transfer at high speeds at reasonable altitudes is aerodynamic heating and it is investigated here in the continuum flow region. The heating analysis is restricted to simple shapes (cones and flat plates) from which model targets can be constructed. The effects of radiation heat loss as well as heat input by solar and earth radiation are discussed. No account is made of possible internal heat sources or sinks. The laws of radiation are then coupled with the temperature analysis to produce radiation patterns at various conditions. Several approximations are then evaluated and general trends in radiation characteristics with varying conditions are discussed. The entire discussion is restricted to radiation at the target, and the effects of atmospheric attenuation are not considered.

SECTION II
EMISSION OF INFRARED RADIATION

In beginning this discussion of infrared radiation from heated surfaces it is important that the basic laws and concepts of thermal emission be reviewed. The purposes of this section are, to establish a radiation nomenclature to be used throughout the paper, to establish the basic equations in a form convenient for later use, and to make clear the necessary assumptions and approximations used. The following is a very brief discussion of the spectral and spatial distribution of infrared radiation from an opaque surface as a function of surface characteristics and temperature. For a more complete and comprehensive treatment the reader is referred to standard physics or heat transfer texts such as Refs. 1 and 2.

In discussing infrared radiation use will be made of a "black body" which is perfectly absorbing at all wavelengths—one which reflects or transmits no radiation. As an example, a small aperture in a large cavity in thermal equilibrium satisfies the requirement of perfect absorption, and is thus a "black" surface. For such a surface, Stefan's law states that the total flux (power per unit area) radiated is proportional to the fourth power of the absolute temperature of the surface that is,

$$q_{bb} = \sigma T^4, \tag{2.1}$$

where

q_{bb} = total flux from black body

T = temperature

σ = Stefan-Boltzman constant

A black body is not a good representation of actual surfaces, and to account for this departure from ideal conditions the ratio of the total flux radiated from a real surface at a given temperature, $q(T)$, to the total flux radiated from a black body at the same temperature is defined as the emissivity, $\epsilon(T)$;

$$\frac{q(T)}{q_{bb}(T)} = \epsilon(T)$$

or using (2.1)

$$q(T) = \epsilon(T)\, \sigma\, T^4 \qquad (2.2)$$

This temperature dependent, total hemispherical emissivity is defined using $q(T)$ and $q_{bb}(T)$ evaluated over all wavelengths, and it is assumed that ϵ is constant over the entire spectrum. A more rigorous treatment would include the variation of ϵ with wavelength, a variation which becomes significant when considering gaseous radiation, or radiation from partially transmitting solids. However, this is of less importance in dealing with opaque surfaces of structural material, since the variation of ϵ with wavelength is small and can be neglected in most cases. All surfaces in the following discussions will be considered "grey" (i.e., ϵ not a function of wavelength), but the strong variation of emissivity with temperature must be accounted for. This is probably best done by referring to measurements of emissivity on structural materials made in the temperature region of interest.

Lambert's cosine law describes the spatial distribution of the radiation from an ideally grey surface element. Referring to the

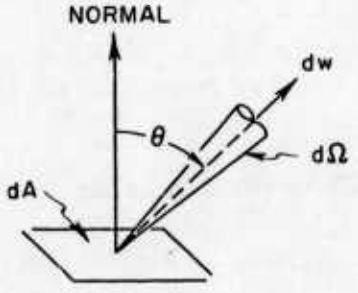

diagram, Lambert's law states that the increment of power, dw, radiating from the element of area dA at temperature, T, into the element of solid angle, $d\Omega$, can be written,

$$dw = \frac{\epsilon \sigma T^4}{\pi} \cos\theta \; d\Omega \, dA, \qquad (2.3)$$

where θ is the angle between the surface normal and the direction of dw. Upon integrating (2.3) over an entire hemisphere, (2.2) is obtained since

$$\frac{dw}{dA} = q .$$

The situation of interest here is one of collecting the surface radiation at long ranges with relatively small apertures. Therefore the solid angle under consideration is very small, so $\cos\theta$ does not vary significantly over Ω and will be assumed constant for any given surface element aspect. Using this assumption, (2.3) is rewritten in the more convenient form of flux (power per unit of radiating surface area) per steradian subtended by the collecting aperture;

$$\frac{dq}{d\Omega} = \frac{\epsilon \sigma T^4}{\pi} \cos\theta \qquad (2.4)$$

Now, (2.4) holds only for a point source, but the assumption of target dimensions much less than the detection range allows the complete target to be considered a point source. The total power of the target as a point source is found by multiplying (2.4) by dA and integrating over the target surface area in view.

$$\frac{dw}{d\Omega} = \int \frac{dq}{d\Omega} \, dA = \frac{\epsilon\sigma}{\pi} \int T^4 \cos\theta \; dA \qquad (2.5)$$

It should be emphasized at this point that Lambert's law as shown in (2.3) and (2.4) holds only for ideally grey surfaces on which ϵ is constant for all observation angles. For real surfaces there is a

disparity in the spatial distribution of radiant energy as the surface is observed from angles near 90° to the surface normal. This variation is best described by allowing the local emissivity to be a function of θ. In dielectric materials this emissivity falls off to a theoretical value of 0 at 90° to the normal. Conductors display an opposite variation; theoretically the emissivity tends to increase as θ approaches 90°. The diagram indicates the nature of the variations by a polar plot of $\epsilon(\theta)$

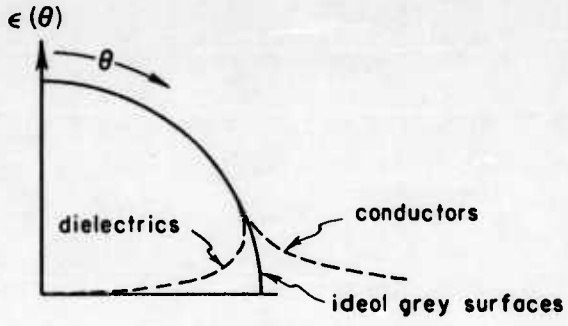

versus θ. These departures from ideal conditions are discussed in some detail in Ref. 2 . However, they will be neglected in this paper for the following reasons. First, the effects are small when the emissivity is relatively high, as it is in normal structural materials. And, second, the correction calculations cannot be made with any degree of accuracy anyway because of the uncertainty in the surface characteristics of a target (smoothness, oxidation, etc.) and the lack of data on the physical characteristics of such surfaces even if they were described (index of refraction for long wavelengths, conductivity, permeability, etc.). Some discretion must be exercised when the line of sight is nearly perpendicular to the surface normal (greater then 75° or 80°), but it can be seen that the results of neglecting the real surface effects tend to be conservative, at least in the case of metallic surfaces.

Up to this point the flux integrated over wavelengths from 0 to ∞ has been considered, however, it is important to know the spectral distribution of the target radiation in order to select sensitive elements and account for atmospheric absorption. The most convenient, continuous description of energy as a function of wavelength utilizes the derivative

of energy with respect to wavelength. If the flux emitted in the wavelength interval between λ and $\lambda + d\lambda$ is defined as $q_\lambda d\lambda$, (or more simply, $q_\lambda = dq / d\lambda$), Planck's law gives the relation;

$$q_{\lambda bb}(\lambda, T)\, d\lambda = \frac{2\pi hc^2}{\lambda^5} \left(\frac{1}{e^{ch/\lambda kT} - 1}\right) d\lambda \quad . \qquad (2.6)$$

This is the basic equation giving q_λ for a black body as a function of wavelength and temperature. Integrating (2.6) from $\lambda = 0$ to $\lambda = \infty$ yields (2.1) with,

$$\sigma = \frac{2\pi^5 k^4}{15\, c^2\, h^3} \quad .$$

In order to obtain a complete description of the radiation from surfaces as a function of temperature, wavelength and geometry (assuming long ranges, relatively small apertures, and ideally grey surfaces) Lambert's cosine law and (2.2) are incorporated into (2.6) to yield,

$$\frac{dq_\lambda}{d\Omega} = \frac{2\, h\, c^2\, \epsilon}{\lambda^5 \left(e^{ch/k\lambda T} - 1\right)} \cos\theta \, . \qquad (2.7)$$

Multiplication of (2.7) by $d\lambda$ and then integration between two wavelengths gives the flux emitted between those two wavelengths per unit solid angle. The form of (2.7) is convenient in that the energy of various targets can be compared directly by evaluation of the right hand side which is independent of range and aperture size. The latter parameters are easily dealt with since,

$$\Omega = A_c / R^2 \quad .$$

The appendix gives a simple way of producing plots of (2.6) or (2.7) for any temperature.

If an analytic expression for $\frac{dq_\lambda}{d\Omega}$ is desired, a great reduction in complexity can be obtained be approximating Planck's equation, (2.7), by Wien's formula. This can be derived from (2.7) by assuming that $ch/\lambda Tk >> 1$ so that the -1 in the denominator can be neglected. This yields

$$\frac{dq_\lambda}{d\Omega} \approx \epsilon\, 2hc^2\, \epsilon^{-ch/\lambda kT} \cos\theta \qquad (2.8)$$

This approximation holds well when $\lambda T << 1.4$ cm°K.

Now consider a surface radiantly exchanging heat with its surroundings. According to Kirchhoff's law the fraction of incident energy absorbed by an opaque surface is equal to its emissivity. So, denoting the surface under study and the external radiation sources by the subscripts 1 and 2 respectively, the net radiation heat flux from the surface can be written,

$$q = \sigma \epsilon_1 \left[T_1^4 - \Sigma \epsilon_2 k_2 T_2^4 \right] \qquad (2.9)$$

The k's are geometrical factors accounting for the extent and orientation of the external radiation sources. The strongest external sources of radiation in the present heating problem are the atmosphere and the sun. There is, of course, a certain amount of "earthshine"; however, it will be assumed that the intervening atmosphere has absorbed enough of this radiation so that it can be neglected. It has been shown (Ref. 3) that optically thick layers of clear air as well as clouds and haze radiate essentially as a black surface at the ambient air temperature. For air totally surrounding the surface under consideration, the geometrical factor equals one. The solar energy can be accounted for by using the common solar constant and a trigonometric factor to account for the surface's orientation. Explicitly,

$$q_s = \alpha \cos\theta$$

$$\alpha = 0.1395 \text{ watts/cm}^2$$

Now (2.9) can be written to include these two sources of heat;

$$q = \sigma \epsilon_1 \left[T_1^4 - T_{air}^4 - \frac{\alpha}{\sigma} \cos\theta_s \right] \qquad (2.10)$$

Obviously the last two terms in (2.10) can be neglected if the temperature of the surface is high enough.

SECTION III

CONTINUUM FLOW AERODYNAMIC HEAT TRANSFER

In this section the equilibrium temperatures and heat transfer rates of aerodynamically heated surfaces in continuum flow will be investigated. This flow regime embraces the region of "conventional" flight where the air can be considered an isotropic continuum and the long developed laws of fluid dynamics can be applied. The temperatures and heating rates on two simple shapes from which most model targets can be constructed (flat plates and cones) are first considered by relatively sophisticated methods to obtain temperature distributions as a function of distance from the leading edge. Then, less laborious, approximate solutions are presented to obtain an isothermal approximation to the temperature distribution. Since aerodynamic heat transfer is a boundary layer phenomena, the two classes of boundary layer flow are considered, laminar and turbulent.

In the following discussion, when local free stream conditions are referred to, it is to be understood that these are the conditions just outside the boundary layer at the point in question. For the simplest case – the flat plate at zero angle of attack – these are the undisturbed ambient conditions. However, in the case of a flat plate at angles of attack other than zero and in the case of a cone, account must be taken of the changes in temperature, pressure and velocity as the flow passes through a shock wave or an expansion wave. For attached shock conditions, wedge and conical shock solutions such as those appearing in Ref. 4 can be used to find the local Mach number and pressure behind these discontinuities. The fact that the stagnation temperature remains constant through an uncurved shock wave yields local static temperature through the Mach number-temperature relation (again found in Ref. 4). For surfaces at a negative angle of attack, the Prandtl-Meyer expansion method serves the same purpose, and is briefly discussed in the same reference.

To carry out the calculations in this section some of the physical properties of air must be known. The ambient conditions as a function

of altitude must be known, and the properties (viscosity, conductivity, specific heat at constant pressure, etc.) as a function of temperature and pressure are also required A useful source of this information is Ref. 5.

A quantity which tends to appear in most continuum flow heat transfer calculations is the adiabatic wall temperature, T_{aw}. This is the wall temperature at which there is no aerodynamic heat transfer between the wall and the stream. For laminar flow it has been found that,

$$T_{aw_\ell} = T^\circ \left[1 + \frac{\gamma-1}{2} \, Pr^{1/2} \, M^2\right], \tag{3.1}$$

and in turbulent flow, the expression becomes

$$T_{aw_t} = T^\circ \left[1 + \frac{\gamma-1}{2} \, Pr^{1/3} \, M^2\right], \tag{3.2}$$

The adiabatic wall temperature is often found through the use of a recovery factor, r, which is defined

$$r = \frac{T_{aw} - T^\circ}{T_0 - T^\circ} \, . \tag{3.3}$$

The recovery temperature, or adiabatic wall temperature, is the same in either system with $r = Pr^{1/2}$ in laminar flow and $r = Pr^{1/3}$ in turbulent flow.

Laminar Flow Over a Flat Plate

The first analysis of the laminar flat plate used in this section is that developed by Lighthill in Ref. 6. In this analysis the solution for compressible, laminar boundary layer with heat transfer and zero pressure gradient found by Pohlhausen is used. The original solution is restricted to the case of a uniform wall temperature; however, Lighthill modified it to apply to a non-uniform wall temperature by adding a solution to the

heat conduction equation in the boundary layer. The resulting expression for the aerodynamic heat transfer as a function of the distance from the leading edge, x, is,

$$q(x) = 0.339\, K\, Pr^{1/3} \left(\frac{u\rho}{\mu}\right)^{1/2} \left(-x^{-1/4}\right) \int_0^x \frac{T'(x_1)\, dx_1}{\left(x^{3/4} - x_1^{3/4}\right)^{1/3}} \qquad (3.4)$$

where the subscript 1 denotes the variable of integration. Expression (3.4) is set equal to the total radiation heat loss, neglecting back radiation from the surroundings (2.2) and after a great deal of non-dimensionalization and application of boundary conditions, the solution to (3.4) is shown to take the form,

$$T(x) = T_{aw} \left[F(Z)\right]. \qquad (3.5)$$

In this expression,

$$Z = \left(\frac{T_{aw}}{T^*}\right)^3 \left(\frac{x}{\ell}\right)^{1/2}, \qquad (3.6)$$

and the reference temperature, T^*, is given by

$$T^{*3} = \frac{0.678\, Pr^{1/3}\, K}{\epsilon\, \sigma\, K} \left(\frac{u\ell\rho}{\mu}\right)^{1/2} \qquad (3.7)$$

The function F(Z) in (3.5) has been evaluated, and is given by the infinite series,

$$F(Z) = 1 - 1.461\, Z + 7.252\, Z^2 - 46.46\, Z^3 + 332.9\, Z^4 - 2538\, Z^5 + 20120\, Z^6 - \cdots \qquad (3.8a)$$

for $Z < .1$, and for $Z > .5$,

$$F(Z) = 0.8409\, Z^{-1/4} - 0.1524\, Z^{-1/2} - 0.0195\, Z^{-3/4} - 0.0038\, Z^{-1} + \cdots \qquad (3.8b)$$

The portion $.1 < Z < .5$ is simply a curve faired between the two solutions since no singularity should exist in that region. The function F(Z) versus Z is shown in Fig. 1. In evaluating the above equations the adiabatic wall temperature, T_{aw}, and the local velocity, u, are

computed for local free stream conditions just outside the boundary layer. The air Prandtl number, Pr, thermal conductivity, K, viscosity, μ, and density, ρ, are evaluated at the wall temperature. The pressure is considered constant throughout the boundary layer. The analysis can be extended to flat plates at angle of attack since there is no pressure gradient over such plates in supersonic flow.

By returning to Pohlhausen's original isothermal wall solution, an approximate temperature for the plate can be obtained. The engineering approach of a heat transfer coefficient, h, and a temperature difference, or temperature potential, is used to estimate the aerodynamically produced heat flux, i.e.

$$q = h\,(T_{aw} - T) \tag{3.9}$$

For the laminar case the adiabatic wall temperature is given by (3.1), and Pohlhausen, as quoted in Ref. 6, gives the local heat transfer coefficient as a function of the streamwise distance from the leading edge, x, as,

$$h = 0.332\ Pr^{1/3}\ K\left(\frac{u\rho}{\mu x}\right)^{1/2} . \tag{3.10}$$

Again the physical properties of conductivity, viscosity and density are evaluated at the wall temperature; the velocity and adiabatic wall temperature are evaluated at local free stream conditions.

To obtain an average heat input over the length of the plate, (3.9) is integrated over the plate length and divided by the total plate area. Specifically, considering a plate of unit width and a streamwise length ℓ, the right hand side of (3.9) becomes,

$$h_{av}\,(T_{aw} - T) = \frac{\int_0^{\ell} q\,dx}{\int_0^{\ell} dx} = \frac{(T_{aw} - T)}{\ell} \int_0^{\ell} h\,dx \tag{3.11}$$

assuming an isothermal wall ($T \neq T(x)$). Incorporating (3.10) in (3.11) and carrying out the integration yields

$$h_{av} = 0.664\ Pr^{1/3}\ K \left(\frac{\rho u}{\mu \ell}\right)^{1/2} \qquad (3.12)$$

Using (3.12) in (3.9) provides the average heat input which is equated to the net radiation heat loss, (2.10), to obtain a fourth order algebraic equation for the isothermal equilibrium temperature on the flat plate.

Laminar Flow Over a Cone

Supersonic, conical flow is amenable to boundary layer calculations for the same reason as flat plate flow; that is, because along any ray the Mach number and the pressure are constant. Therefore, the preceeding analysis for the laminar flat plate can be used after account has been made for the boundary layer "stretching" as it proceeds downstream to accommodate the ever increasing come diameter. The Mangler transformation can be applied to slender, axi-symmetric bodies to transform the three-dimensional flow into an equivalent flow in two dimensions. In Ref. 7 Covert shows that the Lighthill type of solution for conical flow is of the same form as that for the flat plate. Thus the equilibrium temperature distribution on a cone can be calculated using (3.5), (3.7) and (3.8); however, in this case,

$$Z = \left(\frac{T_{aw}}{T^*}\right)^3 \left(\frac{x}{\ell}\right)^{3/2} \frac{1}{\sqrt{3}} \ . \qquad (3.13)$$

It can be seen that the cone angle influences the temperature distribution only through setting the shock configuration, which in turn determines the local physical properties of the air.

Now, to determine the average heat transfer to a laminar cone, the local heat transfer coefficient will still be based on the results of Ref. 6. The distortion of the boundary layer due to the conical nature of the flow can be accounted for by the Mangler transformation again. In Ref. 8 this transformation is applied, and the heat transfer parameters in the conical flow and equivalent flat plate flow cases can be related

$$\frac{h_{cone}}{h_{flat\ plate}} = \sqrt{3} \qquad (3.14)$$

The local heat transfer coefficient on the cone can be found by substituting (3.10) into (3.14) and evaluating the pertinent gas properties at the local free stream conditions. To determine an average heat transfer coefficient for the cone, an isothermal surface is assumed and the heat transferred to the circumferential element of area at axial position, x, is written

$$q\, dA = (T_{aw} - T)\, h\, 2\pi \sin\delta\, x\, dx \qquad (3.15)$$

where δ is the cone half-angle. Integrating (3.15) over the entire cone length, and dividing by the total surface area times $(T_{aw}-T)$ yields an average heat transfer coefficient;

$$h_{av} = \frac{4}{\sqrt{3}} (0.332)\, Pr^{1/3}\, K \left(\frac{u\rho}{\mu \ell}\right)^{1/2} \qquad (3.16)$$

This is the conical counterpart of (3.12) and is used in the form of (3.9) to represent the average aerodynamic heat input to the cone. As in the exact solution, the cone angle effects the temperature only by adjusting the local free stream conditions.

Turbulent Flow Over a Flat Plate

The phenomenon of a turbulent boundary layer flow does not lend itself to neat solutions of relatively high accuracy because the mechanism of turbulence is not well understood, much less mathematically described adequately. Therefore, this discussion will be limited to a very simple approach to the turbulent boundary layer heat transfer problem with heavy reliance on experimentally observed trends and relations. Again the concept of a heat transfer coefficient and a temperature difference is used; and it is of use to introduce the non-dimensional Stanton number, St, defined as

$$St = h/\rho_\infty u_\infty c_p \tag{3.17}$$

where ρ_∞, u_∞ and c_p are evaluated at local free stream conditions. (The subscripts used here are to avoid confusion with the same properties evaluated at the wall temperature which are of importance later.)

In the absence of reliable heat transfer data over a large enough range of Mach number, the Reynolds analogy of a constant relationship between local Stanton number and local skin friction coefficient is used. In Ref. 9 it is pointed out that this relation is constant over a wide range of altitudes and Mach numbers and can be well approximated by:

$$St = .6\ c_f$$

Using this equation and the friction coefficient data presented in Ref. 9 the ratio of compressible St to incompressible St is plotted in Fig. 2 as a function of Mach number. It is assumed that this curve is not changed significantly with variation in Reynolds number or heat transfer rate.

Based on reasonably sound assumptions about the velocity distribution in the boundary layer, Ref. 10 gives the Stanton number for the incompressible, turbulent boundary layer as

$$St_i = (0.0288)\ \left(\frac{\rho u x}{\mu}\right)^{4/5}\ Pr^{1/3}\ K x^{-1}\ (\rho_\infty u_\infty c_p)^{-1} \tag{3.18}$$

To produce an isothermal approximation to the plate temperature as in the laminar case, the heat transfer rate is integrated over the length of the plate, then divided by the total area. Carrying out this operation on (3.18) yields,

$$St_{i_{av}} = 0.036\ \left(\frac{\rho u}{\mu}\right)^{4/5}\ Pr^{1/3}\ K \ell^{-1/5}\ (\rho_\infty u_\infty c_p)^{-1} \tag{3.19}$$

Adjusting (3.19) by the appropriate Stanton number ratio from Fig. 2, and evaluating ρ, μ and K at the wall temperature yields the average Stanton number and thus the average heat transfer coefficient to be used in (3.9) with the turbulent value of the adiabatic wall temperature.

Turbulent Flow Over a Cone

The Mangler transformation used in the discussion of the laminar cone can be modified to apply in the case of a turbulent boundary layer. In Ref. 8 it gives

$$\frac{St_{cone}}{St_{flat\ plate}} \approx 1.14 \qquad (3.20)$$

as a result. By applying (3.20) to (3.18) the local Stanton number on the cone can be found. Using a procedure like that which produced (3.16), the total heat transferred to the cone is found, assuming an isothermal condition, and then non-dimensionalized to obtain an average Stanton number. This process yields an incompressible equation, based on (3.18),

$$St_{i_{av}} = .03648\left(\frac{\rho u}{\mu}\right)^{4/5} Pr^{1/3} K\ell^{-1/5} (\rho_\infty u_\infty c_p)^{-1}. \qquad (3.21)$$

This expression is corrected for compressibility effects using the local Mach number and Fig. 2 to obtain the heat transfer coefficient for the isothermal approximation. It should be noted that, as in the laminar case, the cone angle controls the temperature only through adjusting the shock configuration and thus the local free stream conditions.

SECTION IV
DISCUSSION OF APPROXIMATIONS AND EXAMPLES

In this section the methods of the preceding two sections are applied to some particular cases to demonstrate the validity of the isothermal approximation, and to show the trends in radiation as some of the aerodynamic parameters are varied. The altitudes and velocities selected for the examples are somewhat arbitrary, however, it is felt that they cover the range of interest. A brief comment on the range of validity of the heat transfer equations seems to be in order here. The theories discussed in Section III are for perfect gas in continuum flow. At high Mach numbers the shock waves produced by blunt cones and plane surfaces at high angle of attack raise the air temperature to a level where the real gas effects must be considered. At gas temperatures above 2000°K the real gas effects become noticeable, and the methods of calculating heat transfer rates for those radiation calculations must be re-examined at temperatures above about 3500°K. The assumptions involved in the continuum flow calculations begin to break down when $M/\sqrt{Re}$ gets larger than about 10^{-2}. It can be seen, however, that the range of validity of the methods discussed here covers Mach numbers up to seven and altitudes well above 100,000 ft.; certainly covering nearly all manned aircraft and nonballistic missiles.

To evaluate the isothermal plate approximation in calculating the radiation from simple surfaces, a laminar, flat plate at zero angle of attack is considered. Assuming an emissivity of one and a length of three meters, the temperatures calculated by the Lighthill method are shown in Fig. 3 for Mach numbers 3.0, 5.0 and 7.0, and at altitudes of 30,000 feet and 70,000 feet. The increasing equilibrium temperatures with increasing Mach number is clearly evident. The lower aerodynamic heat transfer rates at higher altitudes (lower free stream density) show up as decreased equilibrium temperatures. The temperatures found by using the isothermal approximation are indicated on the curves. To get an accurate indication of the distribution and level of the infrared radiation from this plate, the Lighthill solutions for the temperature distributions were divided into a number of small isothermal sections, and the contributions of all of those, for a given

condition, were added together to obtain the total w_λ vs. λ curves. These "exact" results are shown, along with the results obtained by considering the plate to be isothermal, in Fig. 4 for the six conditions under consideration.

These curves show the isothermal approximation to be very satisfactory at the low Mach numbers. At a Mach number of 3.0 the approximation leads to an error of less than 10% in w_λ over the wavelengths of general interest. As the Mach number increases, the relatively high temperature region near the leading edge becomes more important and leads to some error in the approximation at short wavelengths. This can be seen in the curves for Mach 5.0 on the short wavelength side of $w_{\lambda max}$. The total radiation predicted by the isothermal approximation is about 90 percent of the more exact value at the 30,000 feet altitude, and only 80 percent of the exact value at 70,000 ft. At Mach number 7.0, even though the radiation level is well approximated at the long wavelengths (beyond about 4 microns), the short wavelength radiation is not well approximated by the isothermal solution, and the approximation predicts only about 80% and about 66% of the total radiant energy at 30,000 ft and 70,000 ft respectively. This discrepancy is probably not great enough to warrant the additional labor involved in the use of the more exact temperature distribution, unless an accurate description of the spectral distribution of the radiant energy is required for special purposes such as discrimination.

To show directly the effect of changing Mach number and surface emissivity, the same flat plate is considered at an altitude of 30,000 ft. Figure 5 shows the results of calculating the radiation for three values of Mach number and three values of emissivity. As would be expected from the previous discussion, the energy level is raised, and λ_{max} becomes smaller as the Mach number increases (due to an increase in heat transfer coefficient, and consequently a higher surface temperature). The families of curves showing the effects of changing emissivity reveal something rather unexpected — in general, the level of $q_{\lambda max}$ is not proportional to ϵ. At Mach 3.0 when the emissivity is reduced by a factor of two, q_λ at the peak of the curve and in the long wavelengths is reduced by less than a factor of two while q_λ below 3μ remains relatively unchanged. At

Mach numbers 5.0 and 7.0 the 1μ to 10μ radiation level is almost unchanged with changes in emissivity. This unusual effect exists because as the emissivity drops, the surface becomes a less efficient radiator, but the surface temperature rises. At higher values of ϵ (lower surface temperatures) the aerodynamic heat transfer rate is higher [see (3.9)] and consequently the rate of total radiation heat transfer is higher; however, a greater fraction of this heat loss takes place in the longer wavelengths and does not appreciably affect the region from 1μ to 10μ.

When the aerodynamic heat transfer rate is put into equation (2.9) to obtain an expression for the wall temperature, considerable simplification can be obtained by omitting one or more of the radiation terms. In order to estimate the effects of these terms, the equilibrium temperatures on a 3 meter flat plate, having a laminar boundary layer and an emissivity of 0.7 were calculated for a range of Mach number and altitude. The results of these calculations are shown in Fig. 6. In this figure the basic, equilibrium temperature solution, (T_w), against which the others are compared, includes only the radiation heat loss from the surface. The T' represents the equilibrium temperature found assuming other forms of the radiation portion of the heat balance equation. The total infrared radiation from the surface is proportional to the fourth power of the surface temperature, hence the $(T' / T_w)^4$ vs. altitude presentation for various Mach numbers.

If the cooling effects of radiation are neglected (3.9) equals zero and the equilibrium temperature equals the adiabatic wall temperature, T_{aw}. It is obvious from Fig. 6 that this cooling effect must be accounted for in all supersonic flight conditions. The ratio $(T_{aw} / T_w)^4$ ranges from a modest 1.3 to a gigantic 28, with the error becoming more pronounced as both the altitude and speed are increased.

Two approximate curves showing the effects of heat radiated to the surface by the surrounding atmosphere also appear in the figure. The temperature increase over T_w results in a total radiation increase of less than 10% at the very high altitudes, and less than 5% below 80,000 ft. Clearly, this term in the heat balance equation need not be considered except in the most unusual situations.

Under some conditions the heat input due to the sun must be considered. Using the radiation cooling and normal incidence solar radiation terms in the heat balance equations, the third family of curves in Fig. 6 was produced. It can be seen that at low speeds and high altitudes the increased surface temperature due to the sunshine produces a significant increase in the total infrared radiation.

As a final example, demonstrating the application of the methods discussed in this report, a typical aircraft shape will be considered. An airframe of approximately the size and proportions of a supersonic fighter is assumed and the radiation from the skin is calculated for two flight Mach numbers and two altitudes. Figure 7 shows the assumed configuration and it can be seen that the geometry is simply a combination of a cone, cylinders and rectangular flat plates for ease in calculation. It is felt that this simplification of geometry would not significantly affect the results of the analysis of most real aircraft. The surface emissivity is assumed to be 0.7 which is a representative value for most structural materials.

In Fig. 8 the radiation is calculated for flight at Mach 2.0 at 40,000 ft. and three aspects, nose, plan and side. The contributions of the various structural components can be seen. In the nose aspect, the open area of the inlets is represented by a black surface at the free stream recovery temperature. The total target radiation curve is very near that of a gray body equal in area to the projected area of the target aircraft and at some near body temperature. This is true only at low Mach numbers where the isothermal approximation can be used. At high Mach numbers the high temperatures at short distance from leading edges produce large deviations in the radiation curves which are peculiar to each separate component and an over-all approximation can no longer be nade with any confidence. This phenonena is accentuated in the nose aspect, where the wing leading edges become very much hotter than any body mean temperature, and consequently add radiation at the shorter wavelengths.

Figure 9 compares the radiation from the target aircraft at 40,000 ft. and 60,000 ft. and at Mach numbers of 2.0 and 3.0. Increasing the flight Mach number from 2.0 to 3.0 increases the total target radiation by about a factor of five. This is to be expected, of course, because of the increased adiabatic wall temperature. As the altitude is increased from

40,000 ft to 60,000 ft the total radiation level is decreased 20 % to 30.%. There is really no change in the adiabatic wall temperature, but the drop in free stream density causes a drop in heat transfer rate and therefore the radiation cooling becomes more effective.

REFERENCES

1. Smith, Jones, and Chasmar. The Detection and Measurement of Infrared Radiation. Oxford University Press, London, 1957.

2. Jakob, Max. Heat Transfer. Vol. I and II. John Wiley and Sons, Inc., New York, 1949 and 1956.

3. Survey of Sky Radiation Intensities in the Thermal Region. Navord Report 4869, Department of the Navy, Bureau of Ordnance, 1957.

4. Equations, Tables and Charts for Compressible Flow. National Advisory Committee for Aeronautics, Report 1135, 1953.

5. Handbook of Supersonic Aerodynamics. Navord Report 1488, Department of the Navy, Bureau of Ordnance, 1950.

6. Lighthill, J. J. Contributions to the Theory of Heat Transfer through a Laminar Boundary Layer. Proceedings of the Royal Society, Series A, Vol. 202, 1950.

7. Covert, Eugene E. Temperature Distribution on Bodies Flying at High Speeds. A and R Memo 118, Naval Supersonic Laboratory, Massachusetts Institute of Technology, 1954.

8. Notes for a Special Summer Program in Aerodynamic Heating of Aircraft Structures. Department of Aeronautical Engineering, Massachusetts Institute of Technology, 1956.

9. Hill, Jacques A. F. Supersonic Heat Transfer Coefficients for Engineering Use. A and R Memo 110, Naval Supersonic Laboratory, Massachusetts Institute of Technology, 1945.

10. Rubesin, M. W. The Effect of an Arbitrary Surface Temperature Variation Along a Flat Plate on the Convective Heat Transfer in an Incompressible Turbulent Boundary Layer. NACA, TN 2345, 1951.

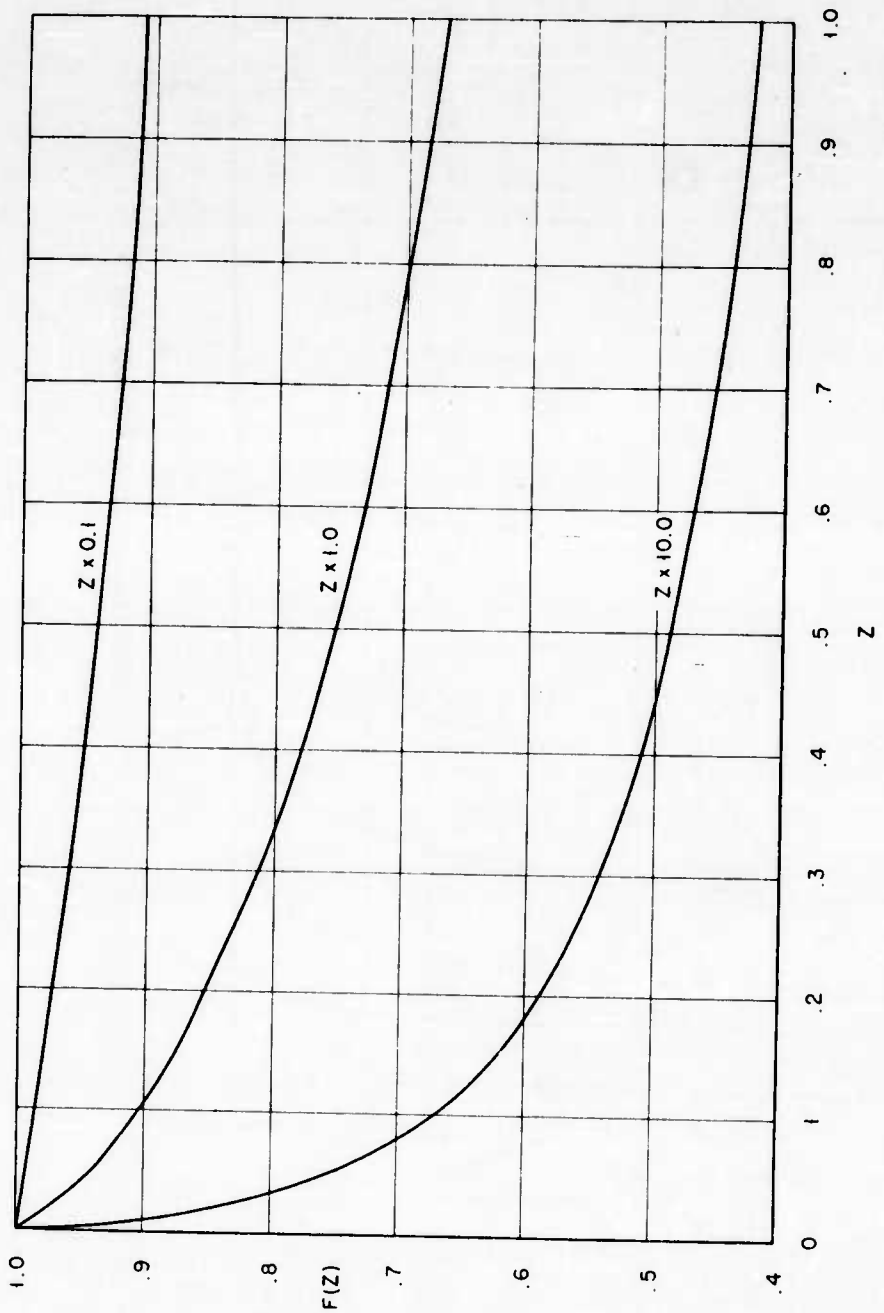

Figure 1. Temperature Decay Parameter, F(Z), versus Nondimensionalized Flat Plate Length, Z, for Laminar Flow.

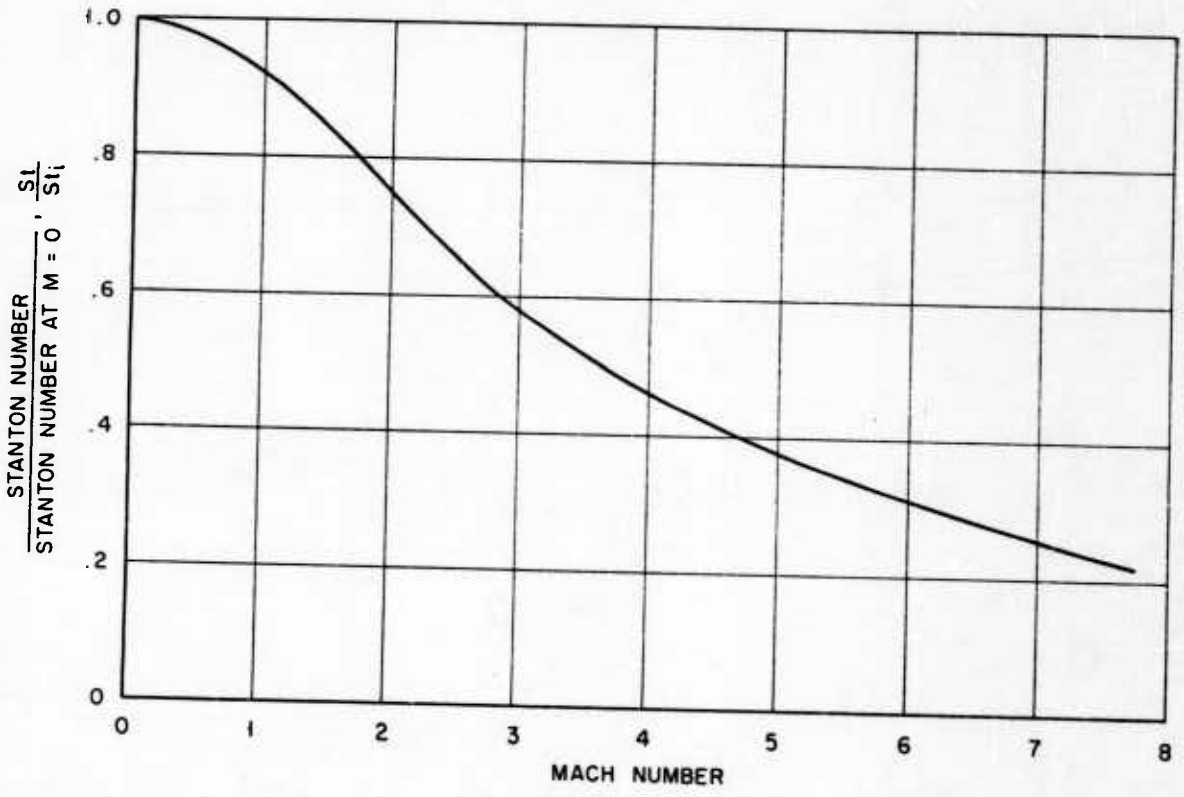

Figure 2. Ratio of Compressible Stanton Number Versus Incompressible Stanton Number versus Mach Number.

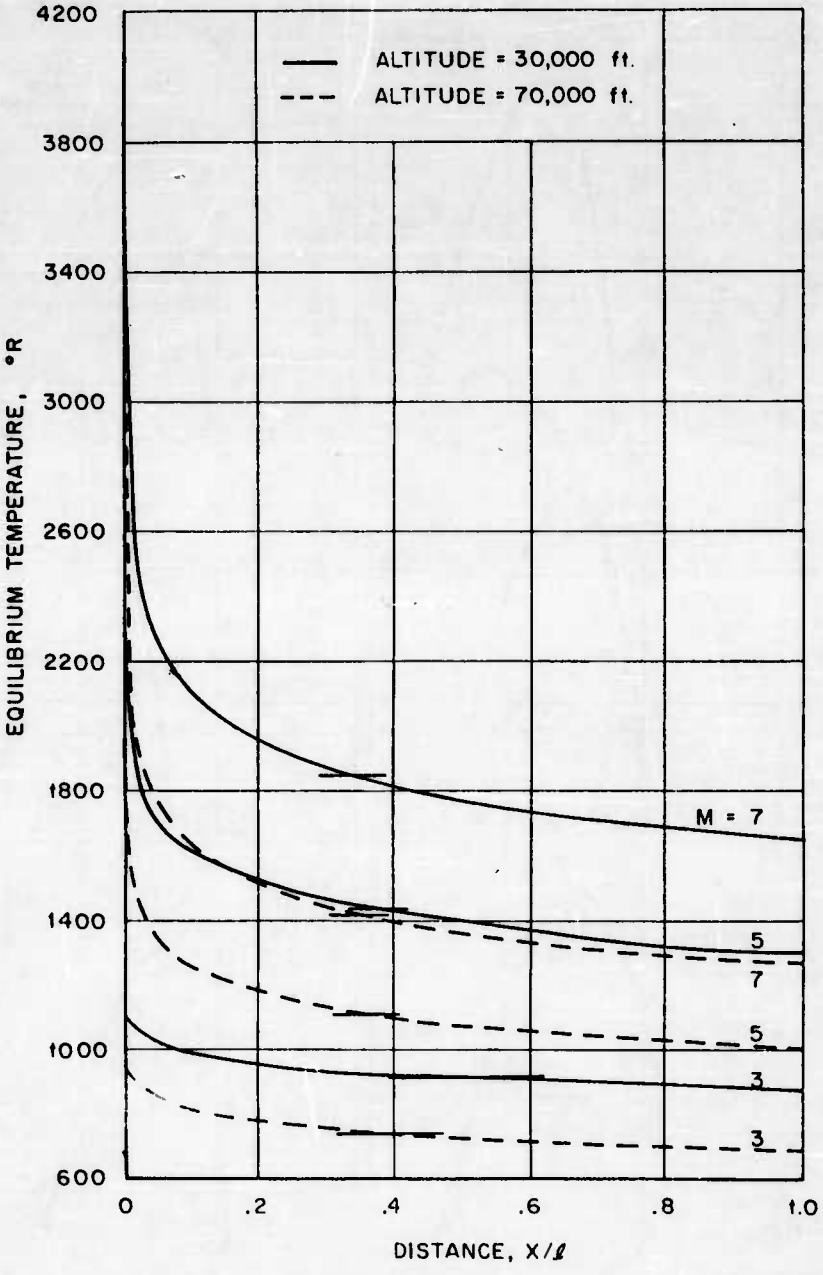

Figure 3. Equilibrium Temperature Versus Distance from Leading Edge, Laminar Flat Plate, $\epsilon = 1$, $\ell = 3$ meters.

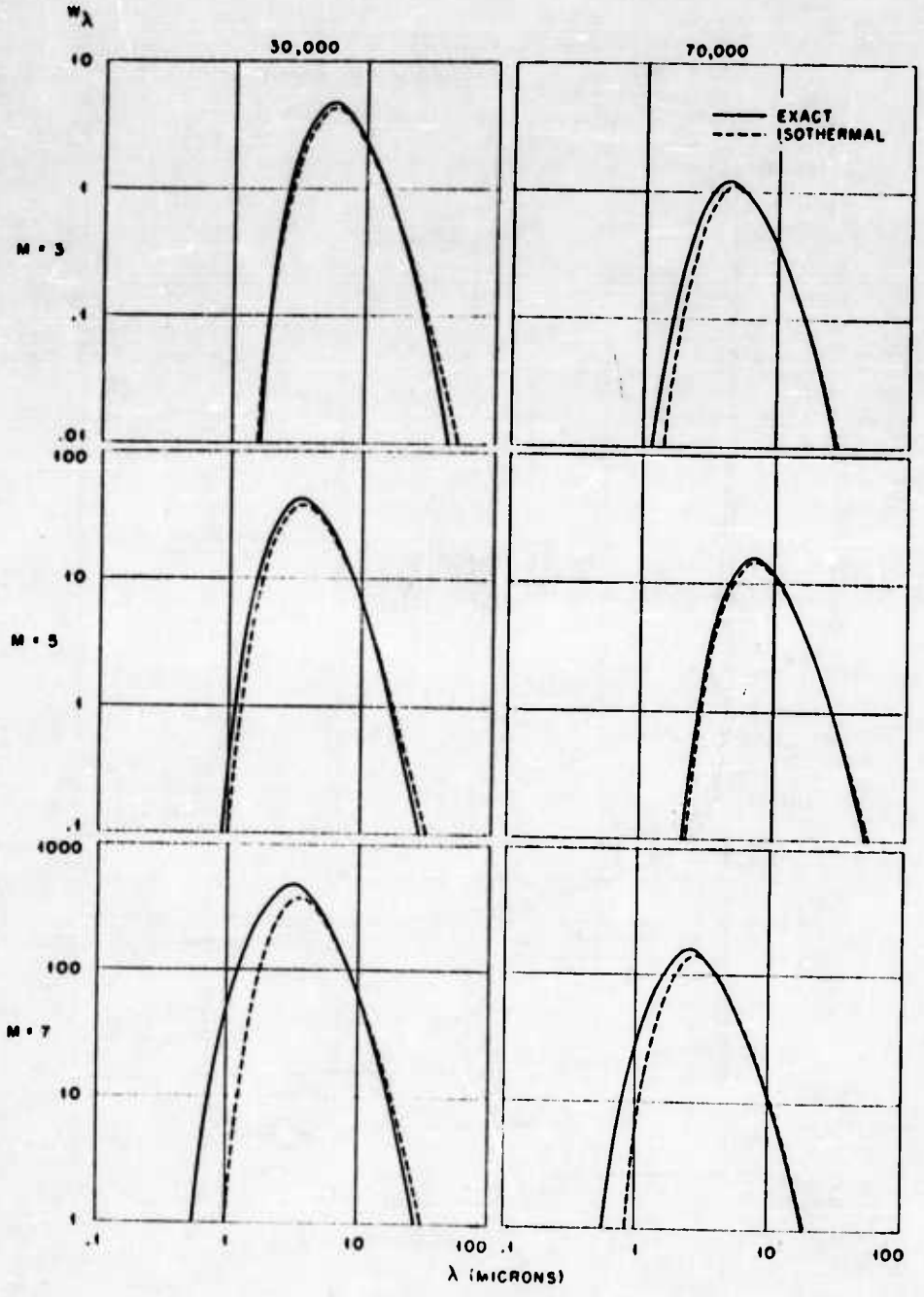

Figure 4. Radiated Power Per Unit Wavelength Versus Wavelength, Laminar Flat Plate, $\epsilon = 1$, $\ell = 3$ meters.

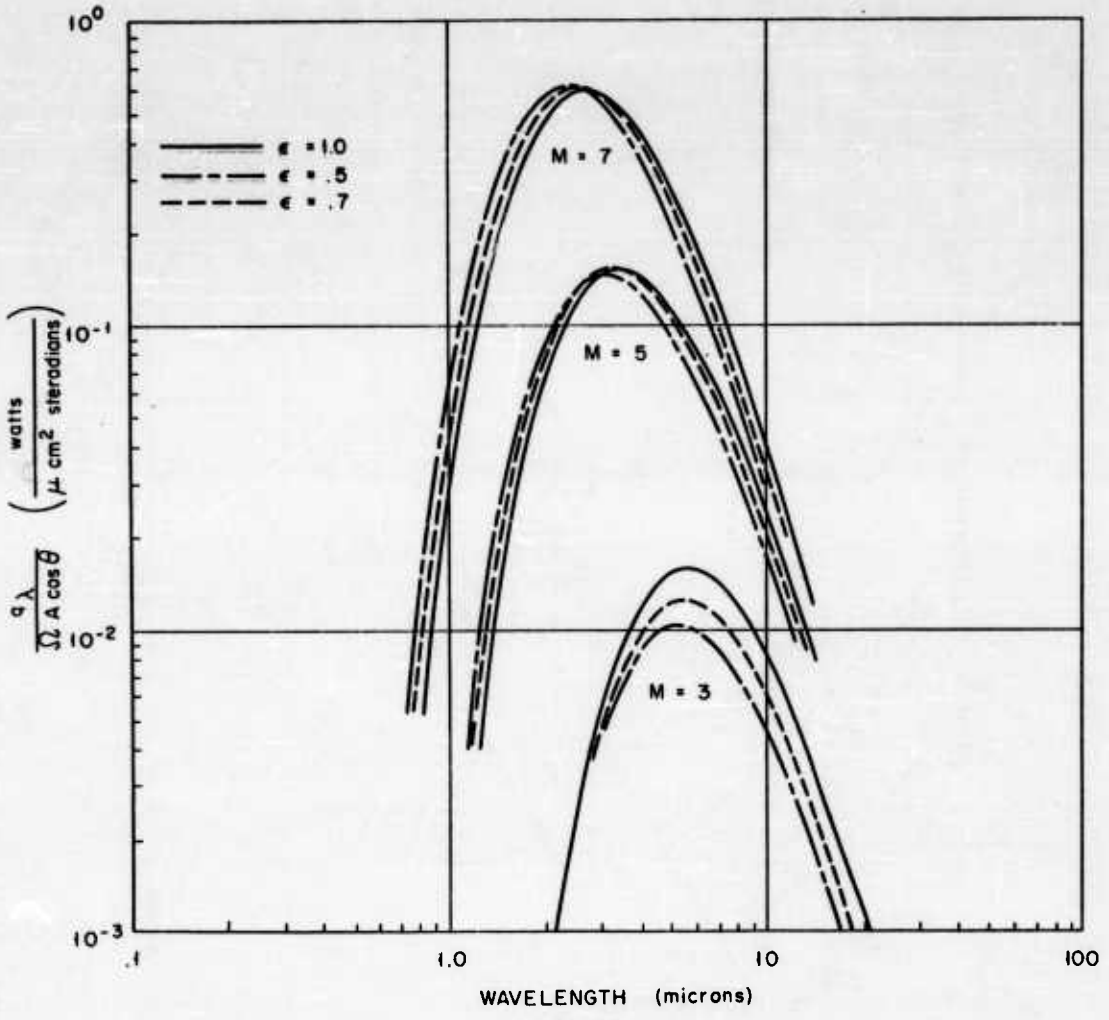

Figure 5. Flux Per Unit Wavelength Versus Wavelength, Laminar Flat Plate at 30,000 ft For Various Mach Numbers and Emissivities. ℓ = 3 meters.

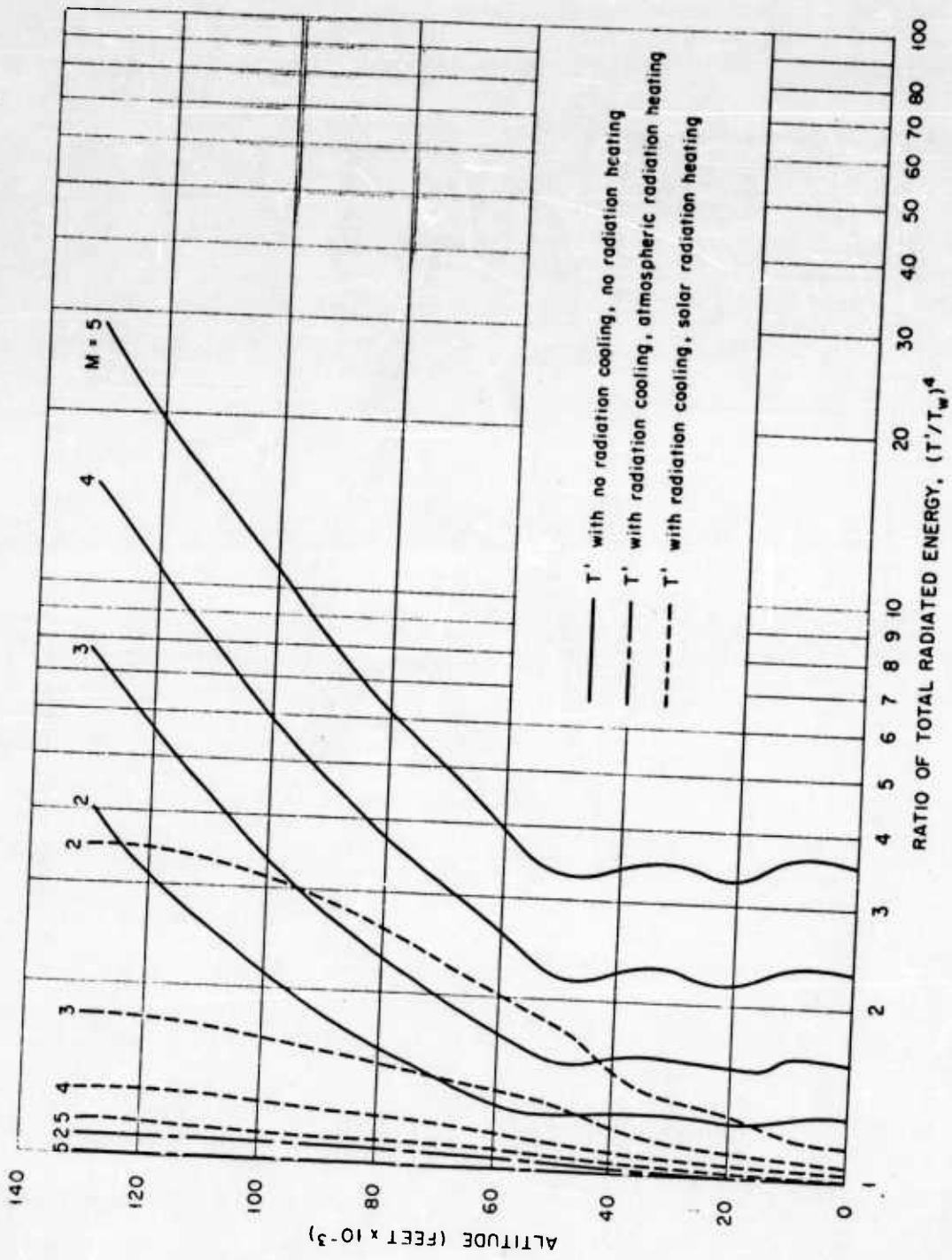

Figure 6. Ratio of Total Radiation Parameters as a Function of Altitude and Mach Number for Various Equilibrium Temperature Approximations.

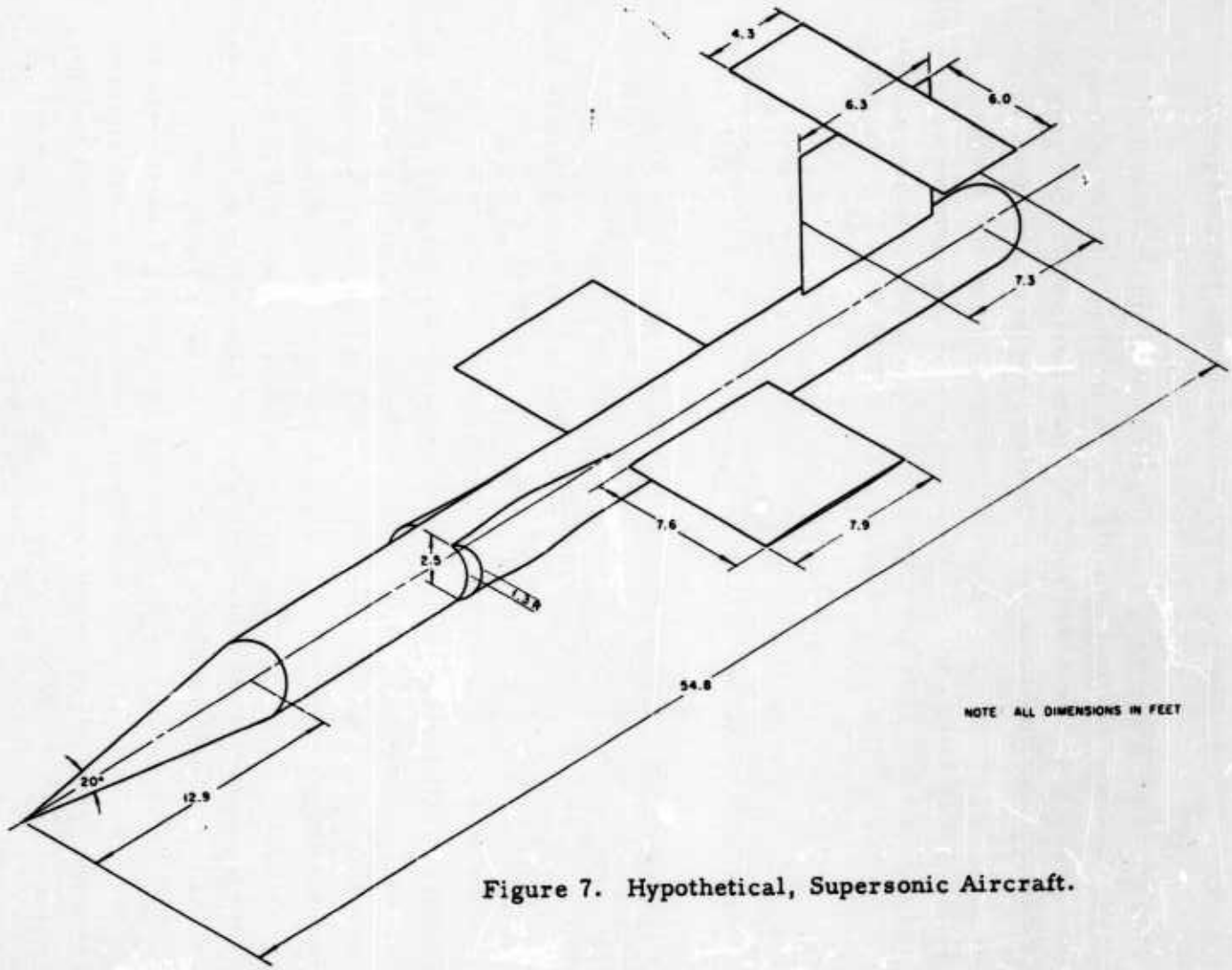

Figure 7. Hypothetical, Supersonic Aircraft.

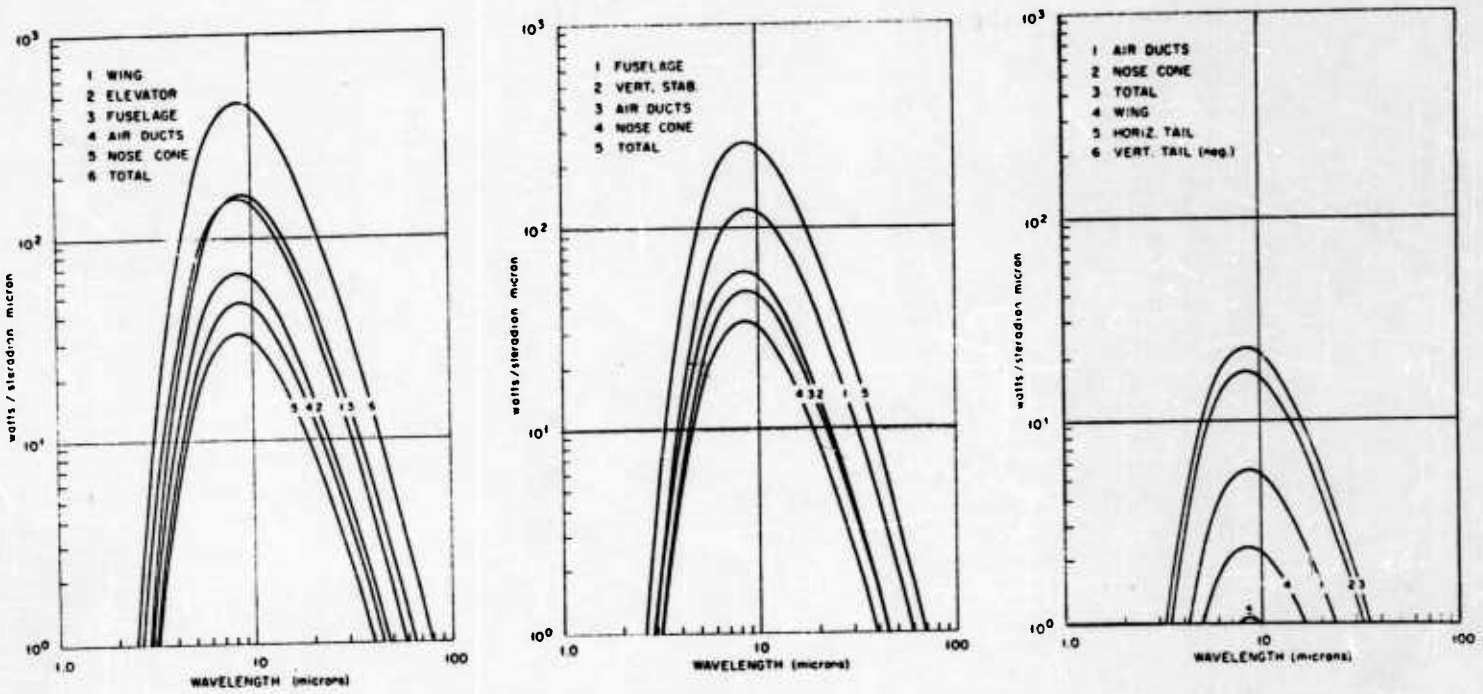

Plan Aspect

Side Aspect

Front Aspect

Figure 8. Radiated Power Per Unit Wavelength and Solid Angle Versus Wavelength, Hypothetical, Supersonic Aircraft M = 2.0, Altitude = 40,000 ft.

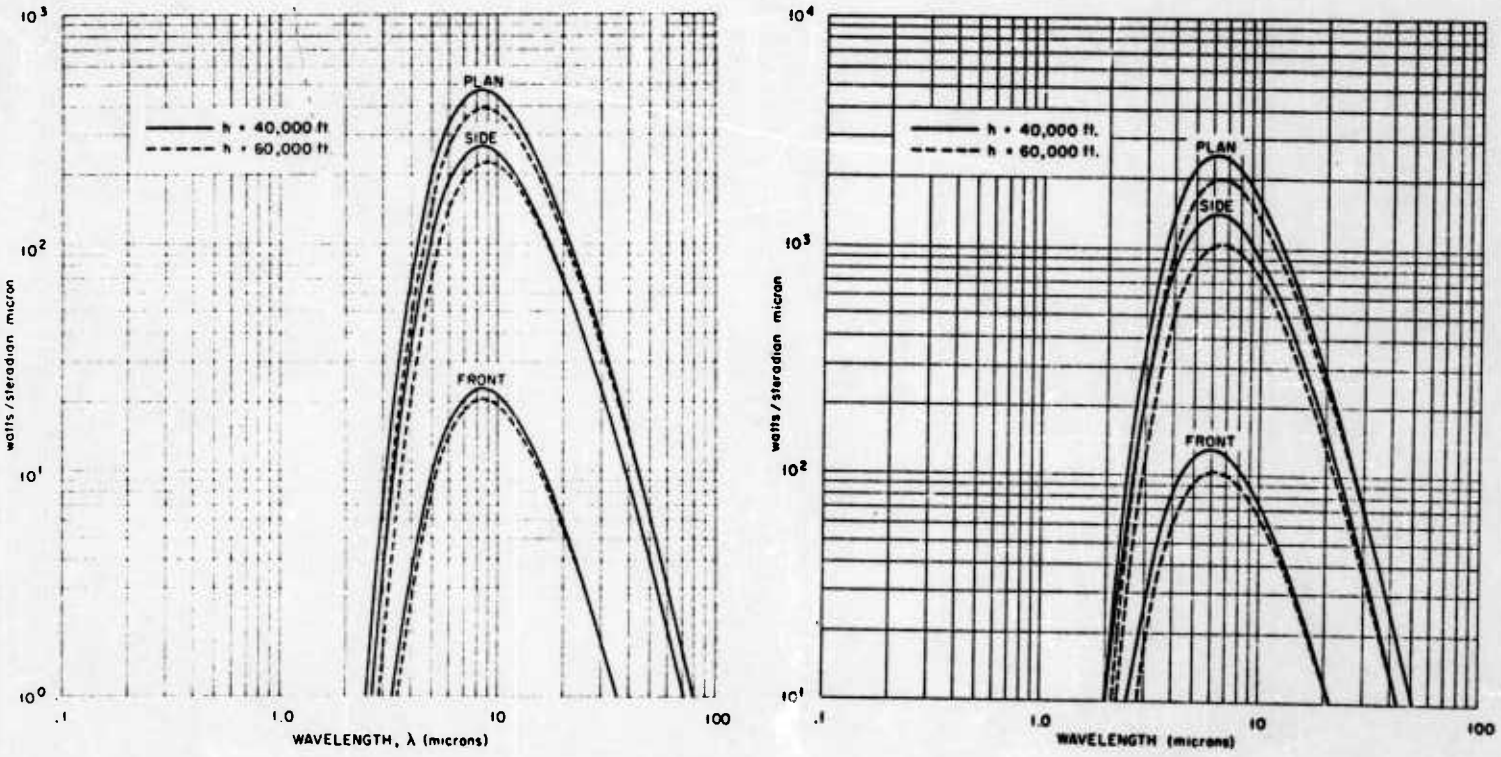

M = 2.0 M = 3.0

Figure 9. Radiated Power Per Unit Wavelength and Solid Angle Versus Wavelength, Hypothetical Supersonic Aircraft.

APPENDIX A
GRAPHICAL PRESENTATION OF PLANCK'S EQUATION

It is desirable to have a simple, rapid method for graphically presenting the flux per unit wavelength as a function of wavelength for any grey body at any temperature. Equation (2.6) is too cumbersome to evaluate for each case and a method is outlined below which allows a plot of q_λ versus λ to be made conveniently.

Considering (2.6), unencumbered by the constants accounting for the geometry and emissivity, Planck's radiation equation can be written

$$q_\lambda = \frac{2h\pi c^2}{\lambda^5} \left(e^{ch/k\lambda T} - 1\right)^{-1} \qquad (A-1)$$

Now, if q_λ and λ are replaced by the variables m and n such that

$$\begin{aligned} q_\lambda &= T^5 m \\ \lambda &= n/T \end{aligned} \qquad (A-2)$$

(A-1) can be written

$$m = \frac{2h\pi c^2}{n^5} \left(e^{ch/kn} - 1\right)^{-1} \qquad (A-3)$$

It can be seen that the variation of m with n is independent of temperature. A curve of m versus n, normalized so that the maximum value of m equals one, is shown in Fig. A-1. To obtain q_λ and λ the transformation (A-2) is used, i.e. the curve of Fig. A-1 is multiplied by the appropriate values of T, m and n. (This just means changing the horizontal and vertical position of the curve on a log-log field without changing its shape)

The relative values of any black body radiation curve can be obtained from Fig. A-1, and if one point on the curve can be determined absolutely the entire spectral distribution is known. The most convenient point to examine is the radiation "maximum" or the point of maximum q_λ. In Ref. 1 the wavelength at which this maximum occurs is given as

$$\lambda_{max} = \frac{hc}{(4.9651)kT} \qquad (A-4)$$

or

$$T\lambda_{max} = 2.898 \times 10^{3} \ ^{\circ}K\mu$$

and the value of q_λ at its maximum is given as

$$q_{\lambda max} = (3.18 \times 10^{2}) \frac{KT^{5}\sigma}{\pi hc} \qquad \text{(A-5)}$$

or

$$\frac{q_{\lambda max}}{T^{5}} = 1.2864 \times 10^{-7} \frac{\text{watts}}{cm^{2} \cdot K^{5} \mu}$$

Thus, with equations (A-4) and (A-5) to determine the appropriate position on the q_λ-λ plot of the radiation maximum, the curve of Fig. A-1 can be laid over the log-log paper and the curve drawn for any black body. Of course the value of $q_{\lambda max}$ can be adjusted to account for emissivity and geometric considerations.

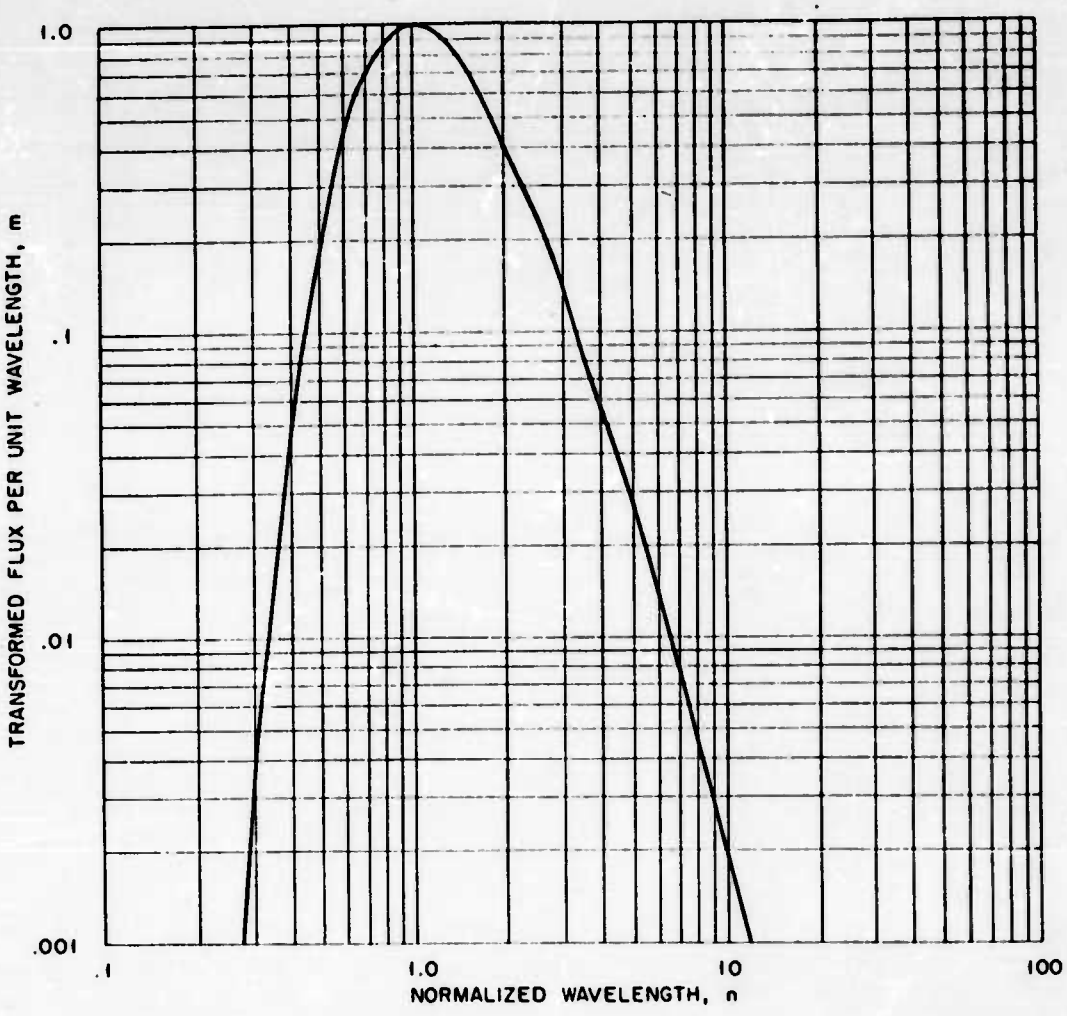

Figure A-1. Transformed Flux Per Unit Wavelength Versus Transformed Wavelength.